nature nanotechnology

REVIEW ARTICLE

PUBLISHED ONLINE: 4 SEPTEMBER 2013 | DOI: 10.1038/NNANO.2013.161

Artificial honeycomb lattices for electrons, atoms and photons

Marco Polini[1]*, Francisco Guinea[2], Maciej Lewenstein[3,4], Hari C. Manoharan[5,6] and Vittorio Pellegrini[1,7]

Artificial honeycomb lattices offer a tunable platform for studying massless Dirac quasiparticles and their topological and correlated phases. Here we review recent progress in the design and fabrication of such synthetic structures focusing on nanopatterning of two-dimensional electron gases in semiconductors, molecule-by-molecule assembly by scanning probe methods and optical trapping of ultracold atoms in crystals of light. We also discuss photonic crystals with Dirac cone dispersion and topologically protected edge states. We emphasize how the interplay between single-particle band-structure engineering and cooperative effects leads to spectacular manifestations in tunnelling and optical spectroscopies.

Graphene is boasting a profound impact in condensed-matter science[1,2] and technology[3–5]. It is an unusually perfect realization of a two-dimensional (2D) semimetal displaying, in a wide range of energies, linearly dispersing conduction and valence bands, which touch at the so-called Dirac point. Charge neutrality pins the Fermi energy at the apex of the Dirac cones, which are particularly intriguing because they imply that quasiparticles behave like relativistic elementary particles with zero rest mass[6].

Dirac conical singularities can emerge in any 2D lattice. In most cases they are anisotropic[7] and require a fine tuning of the parameters that define the lattice[8,9]. Symmetry arguments, however, show that they appear naturally in honeycomb lattices (or, more in general, in lattices with underlying triangular symmetry) at the edges of the Brillouin zone (BZ). Hence, in the search for Dirac fermions in systems other than natural graphene, a good starting point is to study lattices characterized by triangular symmetry.

The extraordinary properties of graphene, ultimately stemming from tunnelling of particles in a honeycomb lattice, have stimulated a number of researchers to realize 'quantum simulators' of graphene and related materials in other systems. These have the advantage of a larger degree of control, may offer fundamental insights on the behaviour of Dirac fermions and, perhaps, provide hints for future developments and applications in technology.

Here we review recent experimental and theoretical advances in the realization of 'artificial graphene' (AG), or more precisely, artificially prepared hexagonal or hexagonal-like lattices. There are many reasons to study such artificial systems. (i) In most of the systems we discuss in this Review, the main effort is to design and control tunnelling of electrons, atoms and photons in a designed hexagonal or hexagonal-like lattice. This allows regimes of parameters that are not accessible in natural graphene to be reached. A paradigmatic example is the regime of strong spin–orbit coupling, which is easy to reach in AG, but is not accessible in natural graphene. (ii) In AG interparticle interactions can be largely controlled by a variety of means, either by controlling the type of particles and their density or by applying external optical or magnetic schemes. One can therefore switch continuously from weak to strong interparticle interactions. In certain systems the role of strong anisotropic dipolar interactions can even be investigated. (iii) Additionally, AG offers the possibility of designing, realizing and studying with local spectroscopy the interplay between Dirac physics and artificial defects. (iv) Finally, in some of the artificial honeycomb systems addressed here, the timescales of dynamics are very long (milliseconds for atoms, for example). This fact provides the unique opportunity to study the dynamical behaviour of many-particle effects *in vivo*, and thus address fundamental questions such as, for instance, persistence of topological states of matter with respect to noise and so on.

Recent advances have demonstrated the possibility of creating AG in diverse subfields of low-energy physics. Current methods of design and synthesis that will be addressed here include (i) nanopatterning of ultrahigh-mobility 2D electron gases (2DEGs)[10–15], (ii) molecule-by-molecule assembly of honeycomb lattices on metal surfaces by scanning probe methods[16], (iii) trapping ultracold fermionic and bosonic atoms in honeycomb optical lattices[17–19], and (iv) confining photons in honeycomb photonic crystals[20–23].

We present an overview of the state of the art of this emerging multidisciplinary field and offer perspectives on possible future developments.

Designing and probing Dirac bands in artificial lattices

Artificial graphene structures offer a playground for comprehending physical phenomena related to the Dirac energy/momentum dispersion relation in regimes that are difficult to achieve in natural graphene. We now discuss the most relevant AG lattices for electrons, atoms and photons explored so far. These systems have complementary physical properties that enable the investigation of a wide range of phenomena.

Figure 1 summarizes four different approaches used to obtain AG and the relevant tunable parameters. It can be argued that whereas the molecular, atomic and photonic analogues of graphene offer an unprecedented control over particle tunnelling, the nanofabricated semiconductor analogue enables the exploration of the impact of long-range interactions and many-body effects. Cold atoms in honeycomb optical lattices offer similar advantages, enriched by the

[1]NEST, Istituto Nanoscienze-CNR and Scuola Normale Superiore, I-56126 Pisa, Italy, [2]Instituto de Ciencia de Materiales de Madrid (CSIC), Sor Juana Inés de la Cruz 3, E-28049 Madrid, Spain, [3]ICFO - Institut de Ciències Fotòniques, Mediterranean Technology Park, Av. Carl Friedrich Gauss 3, E-08860 Castelldefels, Barcelona, Spain, [4]ICREA - Institució Catalana de Recerca i Estudis Avançats, 08010 Barcelona, Spain, [5]Department of Physics, Stanford University, Stanford, California 94305, USA, [6]Stanford Institute for Materials and Energy Sciences, SLAC National Accelerator Laboratory, Menlo Park, California 94025, USA, [7]Istituto Italiano di Tecnologia (IIT), Via Morego 30, 16163 Genova, Italy. *e-mail: m.polini@sns.it

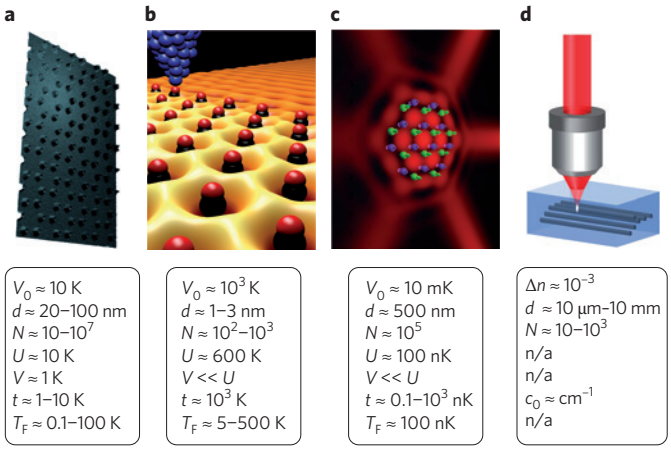

Figure 1 | Artificial graphene structures experimentally obtained by different methods. a–d, Bottom: the main tunable parameters of each approach: V_0 is the lattice depth, d is the lattice constant and N the number of sites. The parameter $U(V)$ is the strength of the on-site (nearest-neighbour) repulsion and t is the single-particle hopping energy. T_F is the Fermi temperature. **a**, Scanning electron micrograph of the surface of a nanopatterned gallium arsenide heterostructure. The distance between two dots is ~130 nm. **b**,**c**, Molecular graphene systems (**b**) and optical lattices for cold atoms (**c**). In panel **b**, red(black) spheres represent the oxygen(carbon) atoms of carbon monoxide molecules whereas the yellow–orange surfaces represent the electron density in a honeycomb pattern. In panel **c**, green and purple spheres represent cold atoms. **d**, Photonic honeycomb crystals made by optical induction methods. Δn is the change of refractive index induced by laser irradiation; c_0 is the coupling constant between waveguides, which plays the role of t. There is no gap in this system except for the one that is induced by strain in the form of Landau levels. Panel **c** courtesy of L. Fallani.

possibility of studying the interplay between many-particle effects and strong spin–orbit coupling on timescales of hundreds of milliseconds. Technologically, however, the semiconductor route to AG offers the key advantage of scalability as silicon and III–V materials are suitable for conventional top-down nanofabrication approaches. The realization of AG in semiconductors requires, however, a fine control over disorder (to the end of minimizing it with respect to for example, inter-site tunnelling), whereas the other analogues of graphene are either disorder free (for example, cold atoms) or characterized by tunnelling energy scales that are substantially larger than disorder (for example, molecules deposited on metals).

Confining electrons. In 1970, Esaki and Tsu realized the possibility of engineering energy bands by artificially modulating the potential in one direction[24]. This pioneering work stimulated a large effort focused on bandgap engineering in semiconductor heterostructures that, thanks to the refinement of nanofabrication techniques, eventually led to the development of lateral superlattices–semiconductor systems characterized by a 2D periodic potential modulation[25].

Exploitation of these artificial crystals started in the late 1980s and enabled the observation of Weiss oscillations[26], chaotic dynamics and Hofstadter butterfly phenomena[27,28]. Similar effects have been recently observed in natural graphene on hexagonal boron nitride[29–31].

High-quality 2D patterns with nanoscale dimensions in semiconductor structures hosting ultrahigh-mobility electrons can be achieved by a combination of electron-beam nanolithography, etching and metallic-gate deposition. This combination yields an external potential landscape with honeycomb geometry that acts as a lattice of potential wells (such as quantum dots) to trap electrons and/or holes. The spatial resolution of these techniques can reach values of a few tens of nanometres or even below. Further improvements in spatial resolution can be obtained by bottom-up nanofabrication methods, for example, by designing semiconductor lattices by nanocrystal self-assembly[32]. These approaches allow to independently control the electron density and inter-site distances and to tune the interplay between on-site (U) and nearest-neighbour (V) repulsive interactions and single-particle hopping energy (t), opening the way to the observation of collective phenomena and quantum phase transitions in such AG solid-state systems.

Recent experimental results obtained in honeycomb patterns defined on 2DEGs in GaAs quantum heterostructures paved the way for the realization of semiconductor AG[11–14]. Experimental results in the regime $U/t >> 1$ reveal[13] unique low-lying collective excitations, such as 'anomalous spin waves', in the inelastic light scattering spectra (as shown in Fig. 5a–c). Although the presence of Dirac fermions has not been experimentally demonstrated yet in these systems, several theoretical studies[10,11,14] indicate that Dirac bands can be designed to occur under realistic conditions. For example, elementary tight-binding calculations suggest that Dirac cones extending for 1 meV can be obtained by tuning the quantum dot spacing to 20 nm, a value reachable by using nanofabrication methods.

A completely different route to realize solid-state AG has been recently followed in ref. 16 (Fig. 2). These authors succeeded in making AG structures with a lattice constant of a few nanometres by placing CO molecules on top of a Cu substrate with the aid of the tip of a scanning tunnelling microscope (STM; Fig. 2a,b). By probing the density of states of the confined electrons through STM measurements (Fig. 2d) and their evolution as a function of an applied pseudo-magnetic field the authors proved the formation of Dirac bands with the characteristic Landau levels of Dirac fermions[2,6]. Although the screening exerted by the bulk states below the 2DEG on the Cu(111) surface makes these 'molecular graphene' structures not the ideal candidates for exploring many-body effects, the large versatility in the atomic design allows unprecedented local control to embed, map and tune the symmetries underlying the 2D Dirac equation. In this system, the authors estimate U/t ~0.5 using known material parameters[16]. Within the Cu system, there is room to increase the strength of effective interactions by reducing t with larger lattices, or else the atomic manipulation scheme may be extended to other substrates with lower screening effects in a quest to realize interacting phases.

The band structure of molecular graphene can be understood by assuming that the superlattice potential created by the CO molecules acts as a weak perturbation on the parabolic band that describes the Cu surface state. The superlattice potential is most effective at changing the parabolic dispersion at the edges of the superlattice BZ. Results of such a perturbative calculation are shown in Fig. 2c. The superlattice potential hybridizes the six unperturbed Cu surface states, which lie at the corners of the new BZ. The effective Hamiltonian at each corner of the BZ is given by a 3 × 3 matrix, which gives rise to a doublet (blue and green bands in Fig. 2c) and a singlet (red band in Fig. 2c). The doubly degenerate state leads to an effective Dirac equation. This 'nearly free' electron scheme can be generalized to include the effects of strain[16] and spin–orbit coupling[33]. Similar approaches can be applied to describe Dirac bands in AG in semiconductors[10,11]. The general symmetries of the triangular lattice uniquely determine these couplings, which have the same form as graphene[34,35]. In particular, spatially patterning the hopping by means of STM atom manipulation allows the generation of both gauge (pseudo)electric and (pseudo)magnetic fields (Fig. 2e,f). Global changes in the lattice constant in molecular graphene add a simple scalar potential to the Dirac Hamiltonian equivalent to an electrical field, which changes the chemical potential or 'doping'[16]. Local changes to the lattice constant engineer a strain introducing a vector potential equivalent to a large perpendicular magnetic field[16,36,37] , here tunable up to 60 T (Fig. 2f). Finally, creating an alternating bond structure in the form of a Kekulé distortion was shown (Fig. 2e) to attach mass to the formerly massless Dirac fermions, akin to the Higgs field[38–40].

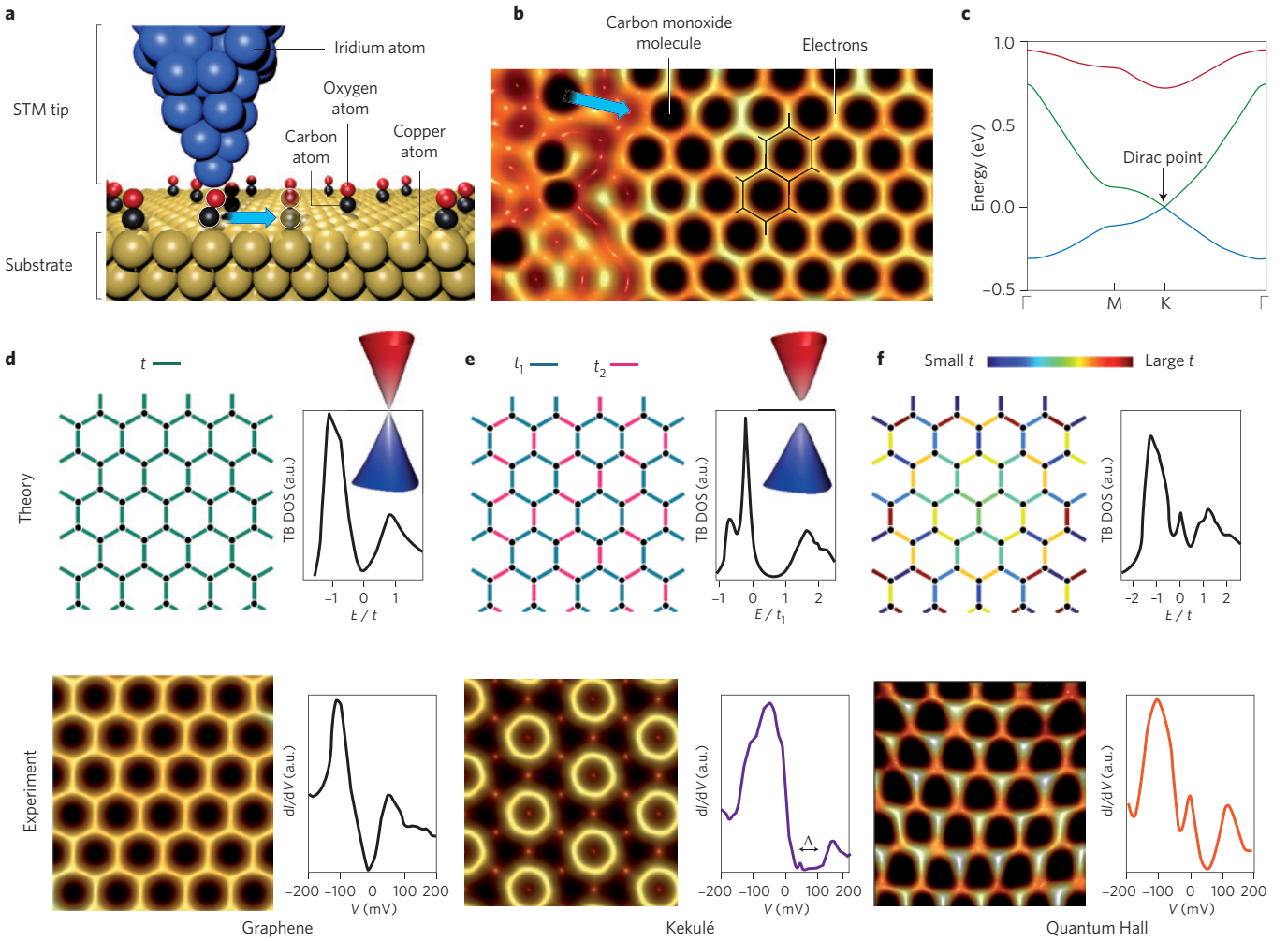

Figure 2 | Designer Dirac fermions in molecular graphene. a, Artificial molecular graphene[16] is fabricated by means of atom manipulation, and then imaged and locally probed by scanning tunnelling microscopy. Carbon monoxide molecules are individually positioned (blue arrow) with the STM tip into a triangular lattice on a copper substrate. The lateral spacing between copper atoms is 2.55 Å. **b**, STM topograph of molecular graphene during assembly, showing 2D surface-state electrons repelled from the molecules and guided into a honeycomb lattice (black lines; blue arrow shows the same as in panel **a**). The lateral spacing between carbon monoxide molecules is 19.2 Å. **c**, Band structure of molecular graphene calculated using the nearly free electron model applied to the periodically perturbed surface electron gas[10]. A Dirac-band crossing appears at the K point of the superlattice BZ. **d**, Pristine quasi-neutral graphene exhibits emergent massless Dirac fermions (d = 19.2 Å, t = 90 meV, t' = 16 meV, where t' is the second nearest-neighbour hopping energy). **e**, Graphene with a Kekulé distortion ($t_1 = 2t_2$) dresses the Dirac fermions with a scalar gauge field creating mass ($0.1 \pm 0.02 m_e$, where m_e is the bare electron mass in vacuum). t_1 and t_2 are the different strengths of the nearest-neighbour hopping energy. **f**, Graphene with a triaxial strain distortion embeds a vector gauge field condensing a time-reversal-invariant relativistic quantum Hall phase (shown here for a large pseudo-magnetic field of 60 T). In the theory panels (top), images are colour representations of the strength of the effective carbon–carbon bonds (corresponding to tight-binding hopping parameters t), and the curves shown are calculated electronic density of states (DOS) from tight-binding (TB) theory. Insets show gapless and gapped Dirac cones matching the experimental data. In the experiment panels (bottom), STM topographs acquired after molecular assembly (100 Å field of view, T = 4.2 K) are shown, and the curves are normalized tunnel conductance spectra obtained from the associated nanomaterial. Figure adapted with permission from: **a**,**b**, ref. 101, © 2012 NPG; **d**–**f**, ref. 16, © 2012 NPG.

For future experiments, the availability of semiconductors (InAs, InSb and so on) and metals (Ag, Au and so on) with large spin–orbit coupling creates concrete and exciting possibilities to explore topological phases of artificial matter with these approaches[11,33,41,42].

Confining photons. Photonic crystals offer an additional route to design energy dispersion relations with characteristic Dirac points[43]. In such crystals, the unusual transmission properties near a Dirac point[20–22] were predicted and observed experimentally.

The state of the art of photonic crystals operating in the microwave frequency range is well described in ref. 44. In this work the crystal is 2D and composed of rows of metallic cylinders, which are arranged to form a triangular lattice. Electromagnetic waves propagating in such a periodic structure, composed of metallic cylinders with radius $R = 0.25\alpha$, where $\alpha \sim 20$ mm is the lattice constant, exhibit a dispersion relation with several Dirac points. In the vicinity of a Dirac point, the measured reflection spectra resemble the STM spectra of graphene flakes[45]. In a subsequent work[46], extremal transmission through a microwave photonic crystal and the observation of edge states close to Dirac points were also demonstrated. The authors of ref. 46 have shown that the transmission through this crystal displays a pseudo-diffusive $1/L$ dependence on the thickness, L, of the crystal. They also measured the eigenmode intensity distributions in a rectangular microwave billiard that contains a

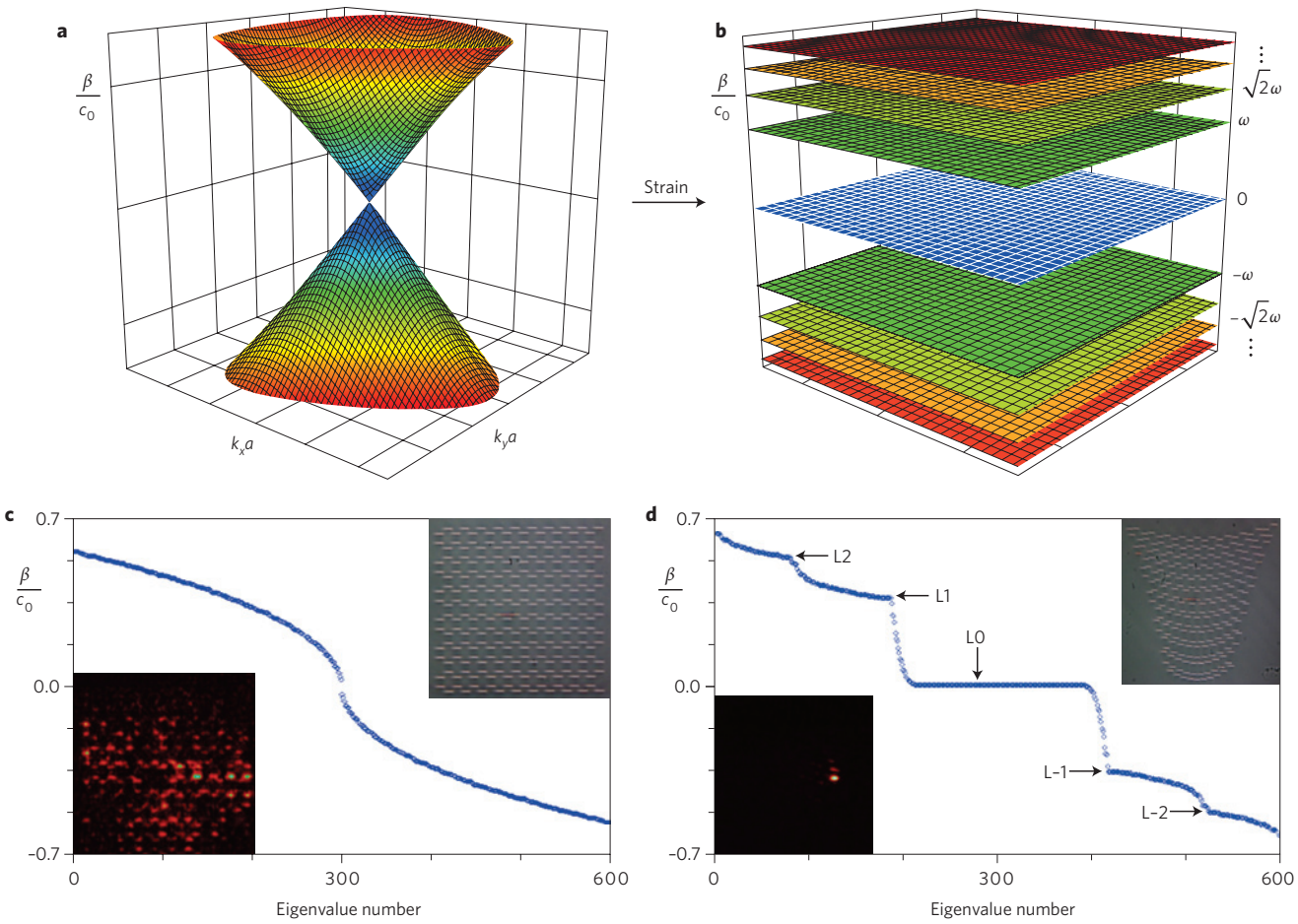

Figure 3 | Landau levels of photons in strained photonic graphene. a, A Dirac cone in the spatial spectrum of unstrained photonic graphene, as obtained by solving equation (1) with the ansatz $\Psi(x,y,z) = \Phi(x,y)\exp(\beta z)$. As in Fig. 1, c_0 plays the role of t. k_x and k_y are the x and y components of the transverse Bloch wavevector **k**, respectively. **b**, Spectrum of inhomogeneously strained photonic graphene, according to a strain tensor that gives a constant pseudomagnetic field. The planes are highly degenerate photonic Landau levels[51]. ω is a numerical factor ~0.37. **c**, Eigenvalues in the unstrained lattice are listed in descending order. Insets show a microscope image of the photonic lattice (top right) and strong diffraction of light through the lattice (bottom left). **d**, Eigenvalues in the strained lattice listed in descending order, showing clear evidence of Landau levels (labelled by Ln with $n = -2, -1, 0, +1, +2$ and so on). Insets show a microscope image of the strained lattice (top right), as well as resulting experimental output showing strong optical confinement in Landau level bandgaps (bottom left). Width of the inset images in **c** and **d** are approximately 0.25 mm. Figure reproduced with permission from ref. 51, © 2013 NPG.

triangular photonic crystal. Close to the Dirac point there appear states at the straight edge of the photonic crystal that represent the artificial counterpart of the states at a zigzag edge of natural graphene. Topological phase transitions of Dirac points in anisotropic honeycomb lattices have also been recently observed[47].

Since 2007, intensive studies of honeycomb lattices constructed by the method of optical induction have been performed. The honeycomb structure in ref. 23 was induced by the intensity pattern $I(x,y)$ of three interfering plane waves, which is translated into a change in the refractive index Δn through the nonlinearity in a photorefractive crystal. Such a lattice exhibits several Dirac points, termed[23] diabolical points after M. V. Berry and M. Wilkinson. The paraxial evolution of the complex amplitude Ψ of a probe beam propagating in the lattice is governed by a Schrödinger-like equation

$$i\frac{\partial \psi}{\partial z} + \nabla_{\perp}^{2}\psi - \frac{V_0\,\psi}{1 + I(x,y) + |\Phi|^2} = 0 \qquad (1)$$

Here, V_0 controls the relative values of potential depth and nonlinearity strength and Φ is defined in Fig. 3 caption. The resulting wave dynamics have been extensively studied[23] offering evidence of the unique phenomenon of conical diffraction (predicted by W. R. Hamilton in the nineteenth century) around the singular diabolical points connecting the first and second bands. Furthermore, 'honeycomb gap solitons', residing in the gap between the second and the third band, were also observed.

In recent years, several theoretical papers were published concerning various aspects of the physics of honeycomb photonic lattices. These include studies of (i) parity and time-reversal symmetry, (ii) nonlinear wave dynamics, (iii) persistence of the Klein effect and (iv) breakdown of conical diffraction due to nonlinear interactions[48,49]. The culmination of these studies has been presented in refs 50–52. Reference 50 describes combined theoretical and experimental work on the creation and destruction of topological edge states in 'optical graphene', where, after the application of uniaxial strain, two Dirac points merge resulting in the formation of a bandgap. Effectively, edge states are created (destroyed) on the zigzag ('bearded') edge of the structure. Moreover, the authors of ref. 50 have claimed the observation of a novel type of bearded edge state, which cannot be explained by the standard tight-binding theory, whereas they can be classified as Tamm states lacking any surface effect. This is an example that highlights how AG structures might provide insights on physics beyond that displayed by natural graphene. A second complementary work[51] demonstrates the creation of synthetic magnetic fields and 'photonic

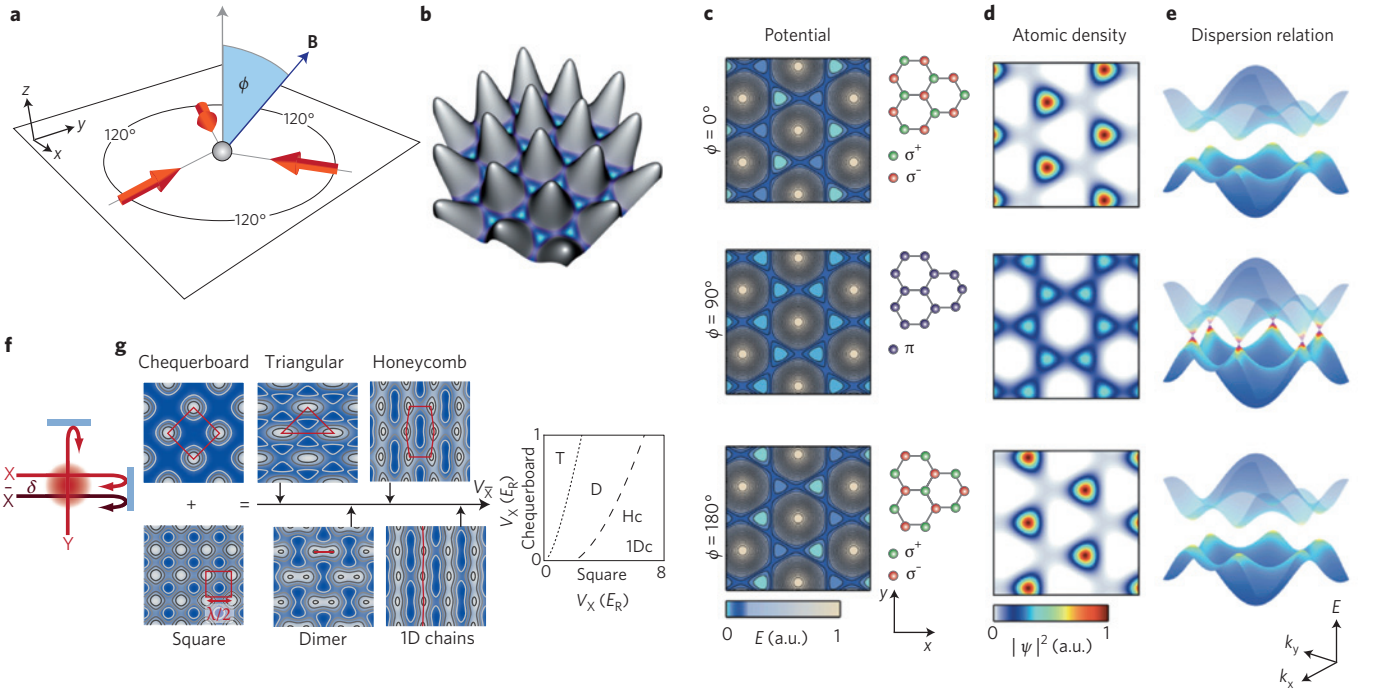

Figure 4 | Flexible optical lattices for cold atom gases. a, Experimental set-up for a spin-dependent hexagonal lattice[18]: three running laser beams intersect (grey sphere) at an angle of 120° with respect to each other. The magnetic field **B** forms an angle ϕ with the z axis. **b**, Resulting scalar potential in the dipole approximation. **c**, Left: the total potential for ^{87}Rb atoms in the Zeeman state $|F = 1; m_F = +1\rangle$ is plotted for $\phi = 0°$, 90° and 180°. m_F is a label for the different atomic Zeeman sublevels. Right: the corresponding light polarization on the two sublattices. **d**, Atomic density distributions in the lowest Bloch band of the potentials plotted in **c**. **e**, Dispersion relation of the two lowest-energy bands. The colour map illustrates the curvature of the bands (blue, minimum curvature; red, maximum curvature). The single-particle energy-momentum dispersion relation evolves as ϕ changes from a gapped to a gapless dispersion relation exhibiting Dirac points. Note that the results for $\phi = 180°$ can be obtained from those for $\phi = 0°$ by exchanging minima and maxima of the total potential and atomic density, as well as σ^- (red) and σ^+ (green). k_x and k_y are the x and y components of the Bloch wavevector **k**. **f**, An optical lattice of tunable geometry has been created in ref. 19 by using three retro-reflected laser beams. Beams X and Y interfere and produce a chequerboard pattern, while beam $\bar{X}$ creates an independent standing wave. Their relative position is controlled by the detuning δ. **g**, Different lattices result from the overlap of chequerboard and square patterns. White (blue) regions denote lower (higher) values of the potential energy. The diagram on the right shows the accessible lattice geometries as a function of the lattice depths $V_{\bar{X}}$ and V_X associated with beams $\bar{X}$ and X, respectively. The transition between triangular (T) and dimer (D) lattices is indicated by a dotted line. Dirac points appear in the honeycomb regime (Hc), that is, to the right of the dashed line. The limit $V_{\bar{X}} >> V_X, V_Y$ corresponds to weakly coupled, one-dimensional chains (1Dc). E_R is the so-called recoil energy. Panels **a**–**e** courtesy of M. Weinberg and K. Sengstock. Panels **f**,**g** adapted with permission from ref. 19, © 2012 NPG.

Landau levels' separated by bandgaps in the spatial spectrum of the structured dielectric lattice (Fig. 3). This is the photonic analogue of the relativistic electron Landau levels observed in strained molecular graphene[16] (Fig. 2f). Finally, a photonic Floquet topological insulator based on an AG structure of helical waveguides, evanescently coupled to one another, has been proposed in ref. 52. Two-dimensional photonic topological insulators based on optical spin–orbit coupling — achieved through the use of a metamaterial composed of split-ring resonators — have been proposed in ref. 53.

Confining atoms and ions. Ultracold atoms are routinely used as efficient quantum simulators of Bose–Hubbard and Fermi–Hubbard models, lattice spin models and so on[54]. In recent years, a great deal of attention has been devoted to quantum simulations involving honeycomb optical lattices with the aim to seek out novel phenomena that are beyond reach in carbon-based 2D honeycomb crystals. Optical lattices are, for example, flexible in the sense that their geometry can be changed *in situ*. Cold atoms in optical lattices, moreover, can be forced into regimes or be subject to external fields, which are difficult to achieve in or inaccessible to natural graphene. Examples include the regime of ultrastrong spin–orbit coupling[55] and non-Abelian gauge fields[56,57] akin to those that appear in the Lagrangian of quantum chromodynamics. Note that with the advent of molecular graphene[16], proposals now also exist for realizing non-Abelian gauge fields in solid-state incarnations[58]. Last, but not least, ultracold gases offer novel means to control the nature, strength and range of interparticle interactions[54].

The authors of ref. 18 have pioneered attempts to create flexible honeycomb lattices. In this work the first realization of an ultracold (^{87}Rb) Bose gas in a spin-dependent optical lattice with hexagonal symmetry was reported. The basic structure of this lattice is detailed in Fig. 4a–e. The interplay between band-structure effects and interactions between atoms leads to interesting many-body physics[18], which will be discussed below. One should stress that Dirac physics was not studied in ref. 18. However, this work represents the first realization of a hexagonal lattice that, if loaded with fermions, can give access to graphene-like physics, but it can also serve to realize[57] topological insulators that use lattice shaking and next-neighbour tunnelling.

The authors of ref. 19 have carried out pioneering work on cold (^{40}K) Fermi gases in honeycomb optical lattices. They have created, moved and merged Dirac points in a tunable honeycomb lattice. More recently, the same authors have studied double transfer through Dirac points in a honeycomb optical lattice[59]. These authors measured the quasi-momentum distribution of the atoms after they sequentially passed through two Dirac points and observed a double-peak feature in the fraction of atoms transferred to the second band (both as a

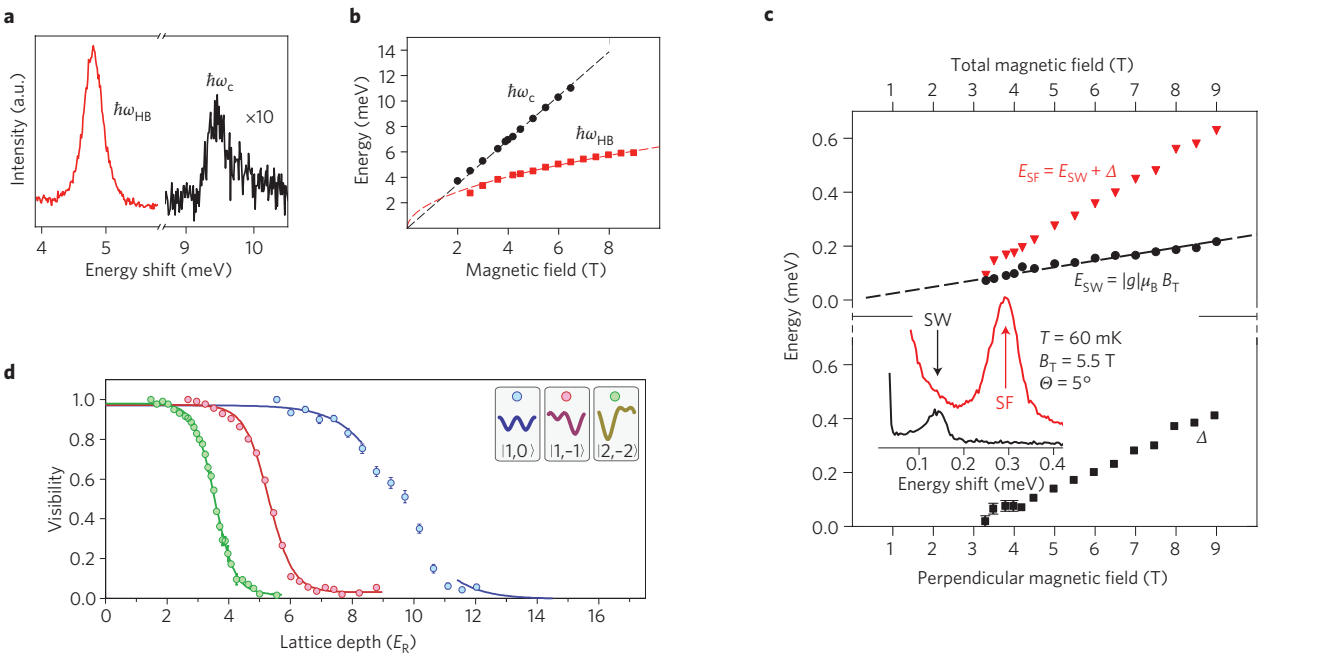

Figure 5 | Many-body effects in artificial honeycomb lattices. a, Resonant inelastic light scattering spectra (at $B = 5.48$ T and $T = 1.7$ K) of a high-mobility 2DEG in the presence of a honeycomb lateral superlattice[13] showing the ordinary cyclotron mode and the Hubbard mode. **b**, Evolution of the energies of the cyclotron mode (black filled circles) and of the Hubbard mode (at frequencies ω_{HB}; red filled squares) at $T = 1.7$ K. The black dashed line is a linear fit to the data, $\hbar\omega_c = \hbar eB/m^*c$) where $m^* = 0.067m_e$. The red dashed line is a fit of the type $\hbar\omega_c = \alpha\sqrt{B}$ where $\alpha \sim 2$ meV. **c**, Energies of two spin collective modes: the ordinary spin-wave mode (black circles) and an anomalous spin-flip mode (red triangles). The black dashed line is a linear fit to the data, $E_{SW} = |g|\mu_B B_T$, with $|g| = 0.42$. Representative excitation spectra of both spin modes at two different laser energies are reported in the inset, B_T is the total magnetic field and Θ the tilt angle of the sample with respect to the magnetic field. The black squares label the splitting Δ between the two spin modes (spin flip, SF; spin wave, SW). **d**, Superfluid-to-Mott-insulator transition in a spin-dependent honeycomb optical lattice[18]. The visibility of the interference fringes in a time-of-flight experiment is plotted as a function of the lattice depth (in units of the recoil energy). At the superfluid-to-Mott-insulator transition the visibility drops down considerably. Data labelled by blue symbols refer to the superfluid-to-Mott-insulator transition in a spin-independent hexagonal lattice, that is, $m_F = 0$. The other two curves refer to finite values of m_F, as indicated in the inset. Figure reproduced with permission from: **a**-**c**, ref. 13, © 2011 AAAS; **d**, ref. 18, © 2011 NPG.

function of the bandgap at the Dirac points and the quasi-momentum of the trajectory). The flexibility of the lattice used in these experiments is illustrated in Fig. 4f,g. The lattice geometry is controlled by tuning the relative intensities of three retro-reflected laser beams, allowing the creation of chequerboard, triangular and honeycomb lattices. In the limit in which one of the lasers has an intensity that is much larger than the other two, a lattice of weakly coupled 1D chains can be realized.

More work on atoms confined in flexible optical lattices will be reviewed in the next section. Trapped ions provide perhaps the best quantum controlled systems available nowadays[60]. Experimental studies on trapped ion systems have focused so far on the simulation of the Dirac equation encoded in motional and internal degrees of freedom of a trapped ion in 3+1 and 1+1 space–time dimensions, and its consequences, such as Zitterbewegung[61] and the Klein paradox[62]. There is, however, a large ongoing effort towards scalable ion systems, using, for instance, arrays of microtraps or self-assembled lattices, where several hundreds of ions in a triangular lattice can be stored[63].

Strong correlations and topological phases

The most interesting phases of matter emerge in systems with a macroscopically large number of degrees of freedom in the presence of interactions. The great advantage of artificial honeycomb lattices is that interactions among electrons, atoms, ions and photons can be engineered and largely tuned. In artificial semiconductor lattices, for example, the kinetic energy can be quenched by applying a magnetic field, thereby emphasizing the role of long-range Coulomb interactions[13]. In ultracold atomic gases, the strength of interactions can be tuned at will by using Feshbach resonances[54,64]. Finally, significant photon–photon interactions can be achieved by utilizing nonlinear optical media, thereby offering the possibility of realizing strongly interacting fluids of light[65].

Hubbard correlations and split bands. The Hubbard model[66] is the cornerstone of the physics of strongly correlated systems. The Hubbard Hamiltonian encodes a daunting competition between t and U (refs 67–69). The single-band Fermi–Hubbard Hamiltonian reads:

$$\hat{\mathcal{H}} = -t\Sigma_{<i,j>,\sigma}(\hat{c}^{\dagger}_{i,\sigma}\hat{c}_{j,\sigma} + \mathrm{Hc}) + U\Sigma_i \hat{n}_{i,\uparrow}\hat{n}_{i,\downarrow} \quad (2)$$

Here $\hat{c}^{\dagger}_{i,\sigma}(\hat{c}_{i,\sigma})$ creates (destroys) a fermion with spin σ at site i of the lattice and $\hat{n}_{i,\sigma} = \hat{c}^{\dagger}_{i,\sigma}\hat{c}_{i,\sigma}$ is the spin-resolved number operator, Hc is the Hermitian conjugate. In the first term, the sum is over all pairs $<i,j>$ of nearest-neighbour sites. A straightforward generalization of equation (2) to the bosonic case exists[70,71].

When interactions are negligible ($U/t \ll 1$), the ground state of the honeycomb-lattice Fermi–Hubbard Hamiltonian is semimetallic with linearly dispersive massless-Dirac-fermion conduction and valence bands touching at two inequivalent points in the BZ. In the non-perturbative regime, $U/t \gtrsim 1$, the ground-state phase diagram of this model has been extensively studied by means of quantum Monte Carlo (QMC) techniques[72]. Early on it was shown that at half filling and for $U/t \gtrsim 5$ a semimetal–Mott insulator transition occurs[73]. Recently, a QMC calculation has demonstrated[74] the existence of a gapped antiferromagnetic phase for $U/t \gtrsim 4.3$ and presented evidence for a gapped spin liquid phase for $3.5 < U/t < 4.3$. The findings of ref. 74 have been recently addressed in ref. 75 that

used QMC simulations of the same model but in larger clusters (containing up to 2,592 sites) and found very weak evidence of a spin liquid phase[75].

An 'extended' Hubbard model involving an additional interaction term describing nearest-neighbour repulsions of strength V has been studied analytically by renormalization-group (RG) techniques in the limit of a large number N_f of fermion flavours[76,77] ($N_f = 4$ for electrons in graphene). It has been found[76,77] that sufficiently large values of V/t stabilize charge-density-wave phases over semimetallic or Mott insulating phases. Numerical RG calculations[78] have qualitatively confirmed these results but have also discovered that second-neighbour repulsions favour states with spontaneously broken time-reversal symmetry (that is, quantum spin Hall phases) over charge- or spin-density waves.

Finally, it has been shown[79] that, when the Fermi energy is moved away from the Dirac point and the system is doped to the vicinity of a van Hove singularity in the density of states (such as the one that occurs at the M point of the honeycomb-lattice band structure[2]), repulsive short-range interactions favour chiral superconductivity over many other competing orderings. An alternative route to non-conventional superconductivity in AG and related compounds relies on the suppression of long-range forces, while keeping[80,81] $U/t \sim 1$. We stress that, so far, it is not clear which of the exotic phases mentioned above can be observed experimentally. This is a challenge for future theoretical and experimental work.

Strong correlations leave deep scars on the excitation spectrum of a many-body system. The simplest example is represented by a gapped collective mode between 'Hubbard split bands'. In the strongly correlated or 'atomic' $U/t >> 1$ limit the Fermi–Hubbard model displays two bands[66,82], which are split by the repulsive interaction energy U arising from having two fermions with antiparallel spin on the same site. In the atomic limit it is therefore natural to expect a gapped collective mode in which particles belonging to the lower Hubbard band are cooperatively promoted to the upper Hubbard band. Such a mode has been observed in a Bose–Einstein condensate in a deep 3D optical lattice[83] and, more recently, in a semiconductor artificial honeycomb lattice[13] (Fig. 5). This AG system displays also an anomalous 'spin-flip' mode (Fig. 5c) that could stem from the removal of the sublattice degeneracy due to inter-site Coulomb repulsions[84]. Explorations of Hubbard excitations and anomalous spin-flip modes can be extended to molecular and photonic AG once interactions in these systems are turned on.

A plethora of many-body effects and lattice models can be very effectively simulated by using cold atoms[54]. Although these systems can be easily driven into the strongly correlated regime, they present a few setbacks, mostly in terms of dynamic timescales and thermalization. In ref. 18, the combined effects of the lattice and interatomic interactions led to a forced antiferromagnetic Néel order, in which two spin-components localize at different lattice sites. Coexistence of Mott-insulator- and superfluid-type order leads to the formation of a forced supersolid. Next-nearest-neighbour tunnelling seems to play a role in the physics described in ref. 18, a fact that paves the way for the realization of the famous Haldane model[85]. Later on, the authors of ref. 86 reported the observation of a quantum phase transition to a multi-orbital superfluid phase in an optical lattice. In this unconventional superfluid, the local phase angle of the complex order parameter is continuously twisted between neighbouring lattice sites. The nature of this twisted superfluid quantum phase is an interaction-induced admixture of the p-orbital contributions favoured by the graphene-like band structure of the hexagonal optical lattice used in the experiment.

In ref. 87 various forms of frustrated classical ferromagnetism have been studied by transforming the lattice geometry from square to triangular to an array of linear chains and back. Finally, in a recent experimental work[88] novel instances of quantum magnetism of ultracold fermions have been reported. In this work, short-range magnetic order has been achieved by loading two-component Fermi gases in either a dimerized or anisotropic simple cubic optical lattice. Flexible kagome lattices have been recently studied in ref. 89.

Long-range interactions. Electrons in nanopatterned 2DEGs[13] offer a natural system for studying correlation effects in the presence of long-range Coulomb interactions. The applicability of the Hubbard model to describe these systems is questionable because the long-range tail of the Coulomb interaction is not screened at the neutrality point.

In recent years, several efforts have been made[90,91] to describe electrons moving in a honeycomb lattice and interacting through the non-relativistic Coulomb force. In this case the strength of interactions is measured by the dimensionless parameter[2,6,72], $\alpha_{ee} \equiv e^2/(\varepsilon\hbar v_F)$, where e is the absolute value of the electron's charge, ε is a suitably defined dielectric constant and v_F is the Fermi velocity. This parameter, which formally resembles[72] the quantum electrodynamics fine-structure constant, plays the role of the U/t coupling constant in the Hubbard model[66].

Quantum Monte Carlo calculations predict[91] the occurrence of an excitonic insulating phase at a critical value $\alpha_{ee} \simeq 1.1$ of the coupling constant for $N_f = 4$ fermion flavours. Note that electrons in natural suspended graphene are characterized by $\alpha_{ee} \simeq 2.2$ (because, in this case, $\varepsilon \sim 1$ and $v_F \sim 10^6$ m s^{-1}). Weak-field magneto-transport experiments have been carried out[92] in high-quality suspended samples. No experimental evidence of a gapped phase has been reported so far in nearly neutral natural graphene[92]. The observed behaviour is more consistent with the existence of a strong renormalization of v_F (ref. 92) and an RG flow towards weak coupling. When the system is doped away from the neutrality point, screening kicks in and the electron fluid behaves as a Fermi liquid, albeit with a number of intriguing twists[72,93,94].

Electrons in artificial honeycomb lattices therefore offer the unique opportunity for studying strong correlation effects, which are beyond reach in natural graphene. The role of long-range electron–electron interactions in AG has been studied by means of density functional theory in ref. 95. Electron–electron interactions have been demonstrated[95] to shift the threshold for the emergence of isolated Dirac points to larger well depths than found without the interactions[10,11]. This effect is particularly pronounced when the number of electrons per well is increased.

Long-range interactions can nowadays also be studied in the realm of atomic physics. Experimental advances in cooling atoms with permanent dipole moments and polar molecules have indeed made it possible to study quantum gases with dipolar interactions. More experimental and theoretical details can be found in recent review articles[96,97].

Summary and perspectives

In this Review we have discussed recent progress in the creation of AG focusing on nanopatterning of high-mobility 2DEGs in semiconductors, molecule-by-molecule assembly via scanning probe methods, confining photons in dielectric crystals and optical trapping of cold atoms in crystals of light. Lattices of superconducting circuits[98] may also offer further opportunities for studying strongly correlated phases of light in honeycomb structures. Furthermore, fully tunable plasmonic analogues of graphene can be realized in 2D honeycomb lattices of metallic nanoparticles[99].

The occurrence of fragile interaction-induced broken-symmetry states in AG might be pre-empted by external unwanted random potentials, which induce inhomogeneities in the particle-number distribution. Controlled sources of disorder can, however, be exploited to investigate the interplay between disorder and interactions[100], and the occurrence of 'Bose glass'[70] phases.

Finally, we foresee useful applications of AG for the realization of new topological phases of matter, and the engineering of Abelian and non-Abelian gauge fields.

Received 12 April 2013; accepted 17 July 2013;
published online 4 September 2013

References

1. Novoselov, K. S. & Geim, A. K. The rise of graphene. *Nature Mater.* **6,** 183–191 (2007).
2. Castro Neto, A. H., Guinea, F., Peres, N. M. R., Novoselov, K. S. & Geim, A. K. The electronic properties of graphene. *Rev. Mod. Phys.* **81,** 109–162 (2009).
3. Bonaccorso, F., Sun, Z., Hasan, T. & Ferrari, A. C. Graphene photonics and optoelectronics. *Nature Photon.* **4,** 611–622 (2010).
4. Novoselov, K. S. *et al.* A roadmap for graphene. *Nature* **490,** 192–200 (2012).
5. Grigorenko, A. N., Polini, M. & Novoselov, K. S. Graphene plasmonics. *Nature Photon.* **6,** 749–758 (2012).
6. Katsnelson, M. I. *Graphene: Carbon in Two Dimensions* (Cambridge Univ. Press, 2012).
7. Goerbig, M. O., Fuchs, J.-N., Montambaux, G. & Piéchon, F. Tilted anisotropic Dirac cones in quinoid-type graphene and α-(BEDT-TTF)$_2$I$_3$. *Phys. Rev. B* **78,** 045415 (2008).
8. Asano, K. & Hotta, C. Designing Dirac points in two-dimensional lattices. *Phys. Rev. B* **83,** 245125 (2011).
9. Lim, L. K., Fuchs, J.-N. & Montambaux, G. Bloch-Zener oscillations across a merging transition of Dirac points. *Phys. Rev. Lett.* **108,** 175303 (2012).
10. Park, C. H. & Louie, S. G. Making massless Dirac fermions from a patterned two-dimensional electron gas. *Nano Lett.* **9,** 1793–1797 (2009).
This article presents the first theoretical analysis and prescription by means of nearly free electron perturbation theory for realizing massless Dirac fermions in patterned semiconductors.
11. Gibertini, M. *et al.* Engineering artificial graphene in a two-dimensional electron gas. *Phys. Rev. B* **79,** 241406(R) (2009).
This article presents the first theoretical analysis based on plane-wave methods of the formation of Dirac bands in a patterned semiconductor. Photoluminescence data demonstrating the impact of the honeycomb lattice on the electron gas were also reported.
12. De Simoni, G. *et al.* Delocalized–localized transition in a semiconductor two-dimensional honeycomb lattice. *Appl. Phys. Lett.* **97,** 132113 (2010).
13. Singha, A. *et al.* Two-dimensional Mott–Hubbard electrons in an artificial honeycomb lattice. *Science* **332,** 1176–1179 (2011).
This article presents combined theoretical and experimental work on the formation of Hubbard split bands in a 2DEG subject to a honeycomb periodic potential and a perpendicular magnetic field.
14. Nadvornik, L. *et al.* From laterally modulated two-dimensional electron gas towards artificial graphene. *New J. Phys.* **14,** 053002 (2012).
15. Goswami, S. *et al.* Transport through an electrostatically defined quantum dot lattice in a two-dimensional electron gas. *Phys. Rev. B* **85,** 075427 (2012).
16. Gomes, K. K., Mar, W., Ko, W., Guinea, F. & Manoharan, H. C. Designer Dirac fermions and topological phases in molecular graphene. *Nature* **483,** 306–310 (2012).
This article reports the first observation of massless and massive Dirac fermions, their tunable electric and magnetic gauge fields, and the Kekulé distortion in an artificial condensed-matter system.
17. Wunsch, B., Guinea, F. & Sols, F. Dirac-point engineering and topological phase transitions in honeycomb optical lattices. *New J. Phys.* **10,** 103027 (2008).
18. Soltan-Panahi, P. *et al.* Multi-component quantum gases in spin-dependent hexagonal lattices. *Nature Phys.* **7,** 434–440 (2011).
This article represents the first realization of a hexagonal optical lattice for cold atoms; although it deals with bosons, it already shows specific consequences of hexagonal geometry.
19. Tarruell, L., Greif, D., Uehlinger, T., Jotzu, G. & Esslinger, T. Creating, moving and merging Dirac points with a Fermi gas in a tunable honeycomb lattice. *Nature* **483,** 302–305 (2012).
This article presents the first realization of a hexagonal-like lattice and Dirac points for fermions in ultracold atomic lattices.
20. Haldane, F. D. M. & Raghu, S. Possible realization of directional optical waveguides in photonic crystals with broken time-reversal symmetry. *Phys. Rev. Lett.* **100,** 013904 (2008).
21. Sepkhanov, R. A., Bazaliy, Ya. B. & Beenakker, C. W. J. Extremal transmission at the Dirac point of a photonic band structure. *Phys. Rev. A* **75,** 063813 (2007).
22. Sepkhanov, R. A., Nilsson, J. & Beenakker, C. W. J. Proposed method for detection of the pseudospin-1/2 Berry phase in a photonic crystal with a Dirac spectrum. *Phys. Rev. B* **78,** 045122 (2008).
23. Peleg, O. *et al.* Conical diffraction and gap solitons in honeycomb photonic lattices. *Phys. Rev. Lett.* **98,** 103901 (2007).
24. Esaki, L. & Tsu, R. Superlattice and negative differential conductivity in semiconductors. *IBM J. Res. Dev.* **14,** 61–65 (1970).
25. Bernstein, G. & Ferry D. K. Negative differential conductivity in lateral surface superlattices. *J. Vac. Sci. Technol. B* **5,** 964–966 (1987).
26. Weiss, D., von Klitzing, K., Ploog, K. & Weimann, G. Magnetoresistance oscillations in a two-dimensional electron gas induced by a submicrometer periodic potential. *Europhys. Lett.* **8,** 179–184 (1989).
27. Albrecht, C. *et al.* Evidence of Hofstadter's fractal energy spectrum in the quantized Hall conductance. *Phys. Rev. Lett.* **86,** 147–150 (2001).
28. Melinte, S. *et al.* Laterally modulated 2D electron system in the extreme quantum limit. *Phys. Rev. Lett.* **92,** 036802 (2004).
29. Dean, C. R. *et al.* Hofstadter's butterfly and the fractal quantum Hall effect in moiré superlattices. *Nature* **497,** 598–602 (2013).
30. Ponomarenko, L. A. *et al.* Cloning of Dirac fermions in graphene superlattices. *Nature* **497,** 594–597 (2013).
31. Hunt, B. *et al.* Massive Dirac fermions and Hofstadter butterfly in a van der Waals heterostructure. *Science* **340,** 1427–1430 (2013).
32. Evers, W. H. *et al.* Low-dimensional semiconductor superlattices formed by geometric control over nanocrystal attachment. *Nano Lett.* **13,** 2317–2323 (2013).
33. Ghaemi, P., Gopalakrishnan, S. & Hughes, T. L. Designer quantum spin Hall phase transition in molecular graphene. *Phys. Rev. B* **86,** 201406(R) (2012).
34. Kane, C. L. & Mele, E. J. Quantum spin Hall effect in graphene. *Phys. Rev. Lett.* **95,** 226801 (2005).
35. Mañes, J. L. Symmetry-based approach to electron–phonon interactions in graphene. *Phys. Rev. B* **76,** 045430 (2007).
36. Guinea, F., Katsnelson, M. I. & Geim, A. K. Energy gaps and a zero-field quantum Hall effect in graphene by strain engineering. *Nature Phys.* **6,** 30–33 (2010).
This article presents the first theoretical framework for realizing high perpendicular pseudomagnetic fields in graphene by means of strain.
37. Levy, N. *et al.* Strain-induced pseudo-magnetic fields greater than 300 Tesla in graphene nanobubbles. *Science* **329,** 544–547 (2010).
38. Jackiw, R. Fractional charge from topology in polyacetylene and graphene. *AIP Conf. Proc.* **939,** 341–350 (2007).
39. Hou, C.-Y., Chamon, C. & Mudry, C. Electron fractionalization in two-dimensional graphene-like structures. *Phys. Rev. Lett.* **98,** 186809 (2007).
This article is the first theoretical prediction of fractional charge in two dimensions using the Kekulé order parameter.
40. Roy, B. & Herbut, I. F. Unconventional superconductivity on honeycomb lattice: theory of Kekulé order parameter. *Phys. Rev. B* **82,** 035429 (2010).
41. Zhang, Y. & Zhang, C. Quantized anomalous Hall insulator in a nanopatterned two-dimensional electron gas. *Phys. Rev. B* **84,** 085123 (2011).
42. Sushkov, O. P. & Castro Neto, A. H. Topological insulating states in ordinary semiconductors. *Phys. Rev. Lett.* **110,** 186601 (2013).
43. Parimi, P. V. *et al.* Negative refraction and left-handed electromagnetism in microwave photonic crystals. *Phys. Rev. Lett.* **92,** 127401 (2004).
44. Bittner, S. *et al.* Observation of a Dirac point in microwave experiments with a photonic crystal modeling graphene. *Phys. Rev. B* **82,** 014301 (2010).
45. Andrei, E. Y., Li, G. & Du, X. Electronic properties of graphene: a perspective from scanning tunneling microscopy and magneto-transport. *Rep. Prog. Phys.* **75,** 056501 (2012).
46. Bittner, S., Dietz, B., Miski-Oglu, M. & Richter, A. Extremal transmission through a microwave photonic crystal and the observation of edge states in a rectangular Dirac billiard. *Phys. Rev. B* **85,** 064301 (2012).
47. Bellec, M., Kuhl, U., Montambaux, G. & Mortessagne, F. Topological transition of Dirac points in a microwave experiment. *Phys. Rev. Lett.* **110,** 033902 (2013).
48. Szameit, A., Rechtsman, M. C., Bahat-Treidel, O. & Segev, M. PT-symmetry in honeycomb photonic lattices. *Phys. Rev. A* **84,** 021806(R) (2011).
49. Bahat-Treidel, O. *et al.* Klein tunneling in deformed honeycomb lattices. *Phys. Rev. Lett.* **104,** 063901 (2010).
50. Rechtsman, M. C. *et al.* Observation of novel edge states in photonic graphene. Preprint at http://arXiv.org/abs/1210.5361 (2012).
51. Rechtsman, M. C. *et al.* Strain-induced pseudomagnetic field and photonic Landau levels in dielectric structures. *Nature Photon.* **7,** 153–158 (2013).
This article reports the first observation of photonic Landau levels using an artificial dielectric structure.
52. Rechtsman, M. C. *et al.* Photonic Floquet topological insulators. *Nature* **496,** 196–200 (2013).
This article reports the first observation of a photonic Floquet topological insulator, where the propagation direction of light in an artificial system substitutes for the time variable.
53. Khanikaev, A. B. *et al.* Photonic analogue of two-dimensional topological insulators and helical one-way edge transport in bi-anisotropic metamaterials. *Nature Mater.* **12,** 233–239 (2013).
54. Lewenstein, M., Sanpera, A. & Ahufinger, V. *Ultracold Atoms in Optical Lattices: Simulating Many-Body Quantum Systems* (Oxford Univ. Press, 2012).

55. Goldman, N. *et al.* Realistic time-reversal invariant topological insulators with neutral atoms. *Phys. Rev. Lett.* **105,** 255302 (2010).
56. Bermudez, A., Goldman, N., Kubasiak, A., Lewenstein, M. & Martin-Delgado, M. A. Topological phase transitions in the non-Abelian honeycomb lattice. *New J. Phys.* **12,** 033041 (2010).
57. Hauke, P. *et al.* Non-Abelian gauge fields and topological insulators in shaken optical lattices. *Phys. Rev. Lett.* **109,** 145301 (2012).
58. De Juan, F. Non-Abelian gauge fields and quadratic band touching in molecular graphene. *Phys. Rev. B* **87,** 125419 (2013).
59. Uehlinger, T. *et al.* Double transfer through Dirac points in a tunable honeycomb optical lattice. *Eur. Phys. J. Special Topics* **217,** 121–133 (2013).
60. Blatt, R. & Roos, C. F. Quantum simulations with trapped ions. *Nature Phys.* **8,** 277–284 (2012).
61. Gerritsma, R. *et al.* Quantum simulation of the Dirac equation. *Nature* **463,** 68–71 (2010).
62. Gerritsma, R. *et al.* Quantum simulation of the Klein paradox with trapped ions. *Phys. Rev. Lett.* **106,** 060503 (2011).
63. Britton, J. W. *et al.* Engineered two-dimensional Ising interactions on a trapped-ion quantum simulator with hundreds of spins. *Nature* **484,** 489–492 (2012).
64. Duine, R. A. & Stoof, H. T. C. Atom–molecule coherence in Bose gases. *Phys. Rep.* **396,** 115–195 (2004).
65. Carusotto, I. & Ciuti, C. Quantum fluids of light. *Rev. Mod. Phys.* **85,** 299–366 (2013).
66. Hubbard, J. Electron correlations in narrow energy bands. III. An improved solution. *Proc. R. Soc. Lond. A* **281,** 401–419 (1964).
67. Kotliar, G. & Vollhardt, D. Strongly correlated materials: insights from dynamical mean-field theory. *Phys. Today* **57**, 53–59 (March, 2004).
68. Kotliar, G. *et al.* Electronic structure calculations with dynamical mean-field theory. *Rev. Mod. Phys.* **78,** 865–951 (2006).
69. Vollhardt, D. Dynamical mean-field theory of electronic correlations in models and materials. *AIP Conf. Proc.* **1297,** 339–403 (2010).
70. Fisher, M. P. A., Weichman, P. B., Grinstein, G. & Fisher, D. S. Boson localization and the superfluid-insulator transition. *Phys. Rev. B* **40,** 546–570 (1989).
71. Fazio, R. & van der Zant, H. Quantum phase transitions and vortex dynamics in superconducting networks. *Phys. Rep.* **355,** 235–334 (2001).
72. Kotov, V. N., Uchoa, B., Pereira, V. M., Guinea, F. & Castro Neto, A. H. Electron-electron interactions in graphene: current status and perspectives. *Rev. Mod. Phys.* **84,** 1067–1125 (2012).
73. Sorella, S. & Tosatti, E. Semimetal-insulator transition of the Hubbard model in the honeycomb lattice. *Europhys. Lett.* **19,** 699–704 (1992).
74. Meng, Z. Y., Lang, T. C., Wessel, S., Assaad, F. F. & Muramatsu, A. Quantum spin liquid emerging in two-dimensional correlated Dirac fermions. *Nature* **464,** 847–851 (2010).
75. Sorella, S., Otsuka, Y. & Yunoki, S. Absence of a spin liquid phase in the Hubbard model on the honeycomb lattice. *Sci. Rep.* **2,** 992 (2012).
76. Herbut, I. F. Interactions and phase transitions on graphene's honeycomb lattice. *Phys. Rev. Lett.* **97,** 146401 (2006).
77. Herbut, I. F., Juričić, V. & Roy, B. Theory of interacting electrons on the honeycomb lattice. *Phys. Rev. B* **79,** 085116 (2009).
78. Raghu, S., Qi, X.-L., Honerkamp, C. & Zhang, S.-C. Topological Mott insulators. *Phys. Rev. Lett.* **100,** 156401 (2008).
79. Nandkishore, R., Levitov, L. S. & Chubukov, A. V. Chiral superconductivity from repulsive interactions in doped graphene. *Nature Phys.* **8,** 158–163 (2012).
80. Guinea, F. & Uchoa, B. Odd-momentum pairing and superconductivity in vertical graphene heterostructures. *Phys. Rev. B* **86,** 134521 (2012).
81. Roldán, R., Cappelluti, E. & Guinea, F. Interactions and superconductivity in heavily doped MoS_2. Preprint at http://arXiv.org/abs/1301.4836 (2013).
82. Hansen, D., Perepelitsky, E. & Sriram Shastry, B. Split Hubbard bands at low densities. *Phys. Rev. B* **83,** 205134 (2011).
83. Greiner, M., Mandel, O., Esslinger, T., Hänsch, T. W. & Bloch, I. Quantum phase transition from a superfluid to a Mott insulator in a gas of ultracold atoms. *Nature* **415,** 39–44 (2002).
84. Alicea, J. & Fisher, M. P. A. Graphene integer quantum Hall effect in the ferromagnetic and paramagnetic regimes. *Phys. Rev. B* **74,** 075422 (2006).
85. Haldane, F. D. M. Model for a quantum Hall effect without Landau levels: condensed-matter realization of the "parity anomaly". *Phys. Rev. Lett.* **61,** 2015–2018 (1988).
86. Soltan-Panahi, P., Lühmann, D.-S., Struck, J., Windpassinger, P. & Sengstock, K. Quantum phase transition to unconventional multi-orbital superfluidity in optical lattices. *Nature Phys.* **8,** 71–74 (2011).
87. Struck, J. *et al.* Quantum simulation of frustrated classical magnetism in triangular optical lattices. *Science* **333,** 996–999 (2011).
88. Greif, D., Uehlinger, T., Jotzu, G., Tarruell, L. & Esslinger, T. Short-range quantum magnetism of ultracold fermions in an optical lattice. *Science* **340,** 1307–1310 (2013).
89. Jo, G.-B. *et al.* Ultracold atoms in a tunable optical kagome lattice. *Phys. Rev. Lett.* **108,** 045305 (2012).
90. Hands, S. & Strouthos, C. Quantum critical behavior in a graphenelike model. *Phys. Rev. B* **78,** 165423 (2008).
91. Drut, J. E. & Lähde, T. A. Lattice field theory simulations of graphene. *Phys. Rev. B* **79,** 165425 (2009).
92. Elias, D. C. *et al.* Dirac cones reshaped by interaction effects in suspended graphene. *Nature Phys.* **7,** 701–704 (2011).
93. Polini, M., Asgari, R., Barlas, Y., Pereg-Barnea, T. & MacDonald, A. H. Graphene: a pseudochiral Fermi liquid. *Solid-State Commun.* **143,** 58–62 (2007).
94. Barlas, Y., Pereg-Barnea, T., Polini, M., Asgari, R. & MacDonald, A. H. Chirality and correlations in graphene. *Phys. Rev. Lett.* **98,** 236601 (2007).
95. Räsänen, E., Rozzi, C. A., Pittalis, S. & Vignale, G. Electron-electron interactions in artificial graphene. *Phys. Rev. Lett.* **108,** 246803 (2012).
96. Lahaye, T., Menotti, C., Santos, L., Lewenstein, M. & Pfau, T. The physics of dipolar bosonic quantum gases. *Rep. Prog. Phys.* **72,** 126401 (2009).
97. Baranov, M. A., Dalmonte, M., Pupillo, G. & Zoller, P. Condensed matter theory of dipolar quantum gases. *Chem. Rev.* **112,** 5012–5061 (2012).
98. Houck, A. A., Türeci, H. E. & Koch, J. On-chip quantum simulation with superconducting circuits. *Nature Phys.* **8,** 292–299 (2012).
99. Weick, G., Woollacott, C., Barnes, W. L., Hess, O. & Mariani, E. Dirac-like plasmons in honeycomb lattices of metallic nanoparticles. *Phys. Rev. Lett.* **110,** 106801 (2013).
100. Deissler, B. *et al.* Delocalization of a disordered bosonic system by repulsive interactions. *Nature Phys.* **6,** 354–358 (2010).
101. Simon, J. & Greiner, M. A duo of graphene mimics. *Nature* **483,** 282–284 (2012).

Acknowledgements

We thank R. Fazio, M.I. Katsnelson, A. Pinczuk and G. Vignale for very useful discussions. We acknowledge financial support by the Spanish Ministry of Economy (MINECO) through grant no. FIS2011-23713 (F.G.), the European Research Council Advanced Grants 'NOV-GRAPHENE' (F.G.) and 'QUAGATUA' (M.L.), the Spanish Ministry of Science and Innovation (MINCIN) through the grant 'TOQATA' (M.L.), the EU Integrated Project 'AQUTE' (M.L.), the US National Science Foundation through grant DMR-1206916 (H.C.M.), the US Department of Energy, Office of Basic Energy Sciences, Division of Materials Sciences and Engineering, under contract DE-AC02-76SF00515 (H.C.M.), and the Italian Ministry of Education, University, and Research (MIUR) through the programmes 'FIRB - Futuro in Ricerca 2010', grant no. RBFR10M5BT (M.P. and V.P.), and 'FIRB - Futuro in Ricerca 2012', grant no. RBFR12NLNA (V.P.).

Additional information

Reprints and permissions information is available online at www.nature.com/reprints. Correspondence should be addressed to M.P.

Competing financial interests

The authors declare no competing financial interests.